JOURNAL OF THERMOPHYSICS AND HEAT TRANSFER
Vol. 20, No. 4, October–December 2006

Experimental Analysis of Supercritical Startup of Nitrogen/Stainless Steel Cryogenic Heat Pipes

Paulo Couto*
Federal University of Rio de Janeiro, 21945-970 Rio de Janeiro, RJ, Brazil
Marcia B. H. Mantelli†
Federal University of Santa Catarina, 88040-900 Florianopolis, SC, Brazil
and
Jay M. Ochterbeck‡
Clemson University, Clemson, South Carolina 29634-0921

DOI: 10.2514/1.17183

An experimental investigation of the supercritical startup of a nitrogen/stainless steel cryogenic heat pipe is presented. A detailed description of the experimental setup used for this investigation is presented, and several data sets for the transient axial temperature distribution of the heat pipe are shown. A transient, one-dimensional model developed for microgravity environment available in the literature is used to obtain the internal pressure and working fluid axial distribution. The results showed that cryogenic heat pipes are very sensitive to parasitic heat loads (e.g., heat convection), even in rarefied atmospheres, and the parasitic heat loads can significantly change the operational temperature of the cryogenic heat pipe. The effects of parasitic heat loads must be accurately considered during the design stages. Also, the fluid charge plays an important role in the determination of the initial thermodynamic state of the cryogenic heat pipe. An excess of fluid charge may prevent a successful startup due to an increased vapor pressure, whereas a deficiency may prevent the startup due to lack of working fluid to sufficiently prime the heat pipe.

Nomenclature

A	=	area, m^2
A_{wick}	=	cross sectional area of the wick region, m^2
d_w	=	wire diameter, m
k	=	thermal conductivity, W/m · K
L	=	length, m
m	=	mass, kg
m_f	=	working fluid mass, kg
m_{wick}	=	mass of liquid in the wick, kg
N	=	liquid fill ratio
n	=	quality
n_w	=	number of wires
P	=	pressure, kPa
P_{abs}	=	absolute pressure, kPa
P_{vacuum}	=	vacuum chamber pressure, mbar
Q_e	=	evaporator heat load, W
Q_w	=	wire heat leak, W
q_{cond}	=	conduction heat load, W
q_p	=	parasitic heat load, W
s	=	liquid column length, m
T	=	temperature, K
T_i	=	ith thermocouple ($i = 1, 2, \ldots, 27$)
T_{op}	=	heat pipe operational temperature, K
T_{sat}	=	saturation temperature, K
T_0	=	initial temperature, K
V	=	volume, m^3
V_{HP}	=	void volume of the heat pipe, m^3
v	=	specific volume, m^3/kg
v_{HP}	=	specific volume of the working fluid, m^3/kg
x	=	axial coordinate, m
Y	=	measured temperature, K
ΔT	=	temperature difference, K
Δx	=	heat conduction length, m
ε_r	=	absolute random error, K
ε_s	=	absolute systematic error, K
ρ	=	density, kg/m^3
$\varnothing_{\text{int}}$	=	internal diameter, mm

Subscripts

Co	=	constantan
Cu	=	copper
c	=	condenser section
crit	=	critical point thermodynamic properties
ℓ	=	liquid layer, liquid thermodynamic properties
s	=	solid wall, solid thermodynamic properties
sat	=	saturation thermodynamic properties
v	=	vapor layer, vapor thermodynamic properties
w	=	wire

Introduction

HEAT pipes are highly reliable and efficient heat transfer devices considered for many terrestrial and space applications [1,2]. This device uses the latent heat of vaporization (condensation and evaporation) of a working fluid to transfer relatively large amounts of energy over a long distance with a small temperature drop. During normal operation, the working fluid remains in a saturation condition, with liquid contained in a wick structure and vapor in the vapor core section. The saturated liquid evaporates in the evaporator section due to an applied heat load, and the vapor flows towards the condenser section where it condenses on the wick due to heat rejection to a heat sink. The capillary pressure difference developed along the wick structure pumps the working fluid back to the evaporator section.

Presented as Paper 4190 at the 36th AIAA Thermophysics Conference, Orlando, Florida, 23–26 June 2003; received 15 April 2005; revision received 7 March 2006; accepted for publication 3 April 2006.

*Associate Research Engineer; pcouto@lttc.coppe.ufrj.br. Member AIAA.
†Professor; marcia@emc.ufsc.br. Member AIAA.
‡Professor; jochter@ces.clemson.edu. Associate Fellow AIAA.

Cryogenic heat pipes are one of the many different existing types of heat pipes [2], where usually they operate at temperatures below 200 K. Different from low and medium temperature heat pipes, cryogenic heat pipes start from a supercritical condition. The heat pipe must be cooled below the critical temperature of the working fluid for the condensation process to start in the condenser region. A liquid column develops in the wick structure due to the condensation process. As the temperature of the condenser decreases, the liquid column advances towards the evaporator end. The cooling effect of the liquid vaporization at the liquid column leading edge cools the dry length of the heat pipe, priming the wick structure until steady-state operation is achieved [3].

Cryogenic working fluids usually exhibit very low values of surface tension and latent heat of vaporization, resulting in a heat pipe with low heat transport capacities, which are very sensitive to parasitic heat loads [4], fluid charge [5], and acceleration fields [6,7]. The parasitic heat loads can change significantly the operational temperature of the cryogenic heat pipe and may add heat loads to the heat pipe on the order of the maximum transport capability. In addition to imposing additional heat loads, the parasitic heat loads adversely affect the transient startup behavior for the system. Gravitational fields typically help the startup of cryogenic heat pipes as gravity aids spreading of the liquid slug (developed due to excess of working fluid) along the wick structure, assuming the heat pipe is oriented horizontally.

The objective of the present work was to investigate experimentally the startup process of a cryogenic heat pipe accounting for the effects of parasitic heat loads and fluid charge. The effects of acceleration fields have been discussed in the literature [6–8] and will not be repeated here. To achieve the objective of this work an experimental setup was constructed in the Satellite Thermal Control Laboratory (NCTS) of the Federal University of Santa Catarina (UFSC), Brazil, for the ground test of cryogenic heat pipes. A nitrogen/stainless steel cryogenic heat pipe (CryoNHP) was designed and the results of the ground tests are presented. The technology of cryogenic heat pipes is under investigation at NCTS [9] to develop a passive cryogenic thermal control device for payloads of Brazilian satellites [10].

Literature Review

Unlike low and medium temperature heat pipes, a cryogenic heat pipe typically starts from a supercritical state. The entire heat pipe must be cooled below the critical temperature of the working fluid before nominal operation can begin. Previously, Colwell [11], Brennan et al. [12], Rosenfeld et al. [13], Yan and Ochterbeck [3] and Couto et al. [4,14] discussed the startup process of cryogenic heat pipes.

Colwell [11] presented a numerical analysis of the transient behavior of a nitrogen/stainless steel cryogenic heat pipe with a circumferential screen wick structure and composite central slab. The three-dimensional model assumed constant properties, but did not account for the fluid dynamics of the working fluid. Although provisions for simulating a supercritical startup were listed, the author only presented results for the startup of the heat pipe with an initial temperature already below the critical temperature of the working fluid.

A microgravity experiment for two different aluminum/oxygen axially grooved heat pipes was conducted by Brennan et al. [12]. The experiment was flown aboard the STS-53 space shuttle mission in December 1992. Reliable startups in flight of the two heat pipes were performed, but the startup process in microgravity was slower than that obtained in ground tests. This is because in a microgravity environment any excess liquid condensate of the working fluid develops a liquid slug in the condenser region. In ground tests the excess liquid spreads along the top of the wick structure due to the effects of the gravitational forces. In this case, the liquid typically forms a puddle due to the very low surface tension of cryogenic fluids.

Rosenfeld et al. [13] presented a study of the supercritical startup of a titanium/nitrogen heat pipe. The test was performed during mission STS-62 (March 1994). This heat pipe achieved a nonoperational steady-state thermal condition during microgravity tests. Only 30% of the heat pipe length cooled below the nitrogen critical point and the vapor pressure was still above the critical pressure. However, Rosenfeld et al. [13] observed that in ground tests, the titanium/nitrogen heat pipe underwent startup successfully. The authors concluded that, with the addition of parasitic heat loads, the axial thermal conduction of the titanium/nitrogen heat pipe was insufficient to decrease the axial temperature profile to allow for the internal pressure to decrease below the critical pressure of nitrogen when in microgravity. The successful startup during ground tests was due to enhanced thermal transport of the gravity-assisted priming effects. These tests highlighted the significance of the parasitic heat loads, as the heat pipe startup failure would not have occurred in microgravity if the heat leaks had been significantly reduced.

Yan and Ochterbeck [3] presented a one-dimensional transient model for the supercritical startup of cryogenic heat pipes. The startup process was summarized into two stages. In the first stage, the heat pipe is cooled by pure heat conduction, and the vapor temperature at the condenser is greater than the critical temperature ($T_c > T_{crit}$). The cooling effect resulting from the condenser heat rejection is not immediately propagated through the heat pipe, but it is confined to a region extending from the condenser to some penetration depth. Beyond this penetration depth, the temperature gradient is zero. When the penetration depth equals the heat pipe length, the cooling effect of the condenser has propagated over the entire heat pipe.

In the second stage, the vapor temperature is lower than the critical temperature ($T_c < T_{crit}$). When the condenser temperature is lower than the critical temperature and the internal pressure is lower than the critical point, the vapor begins to condense in the condenser section. The advancing liquid layer is subjected to a capillary driving force that is induced by surface tension and opposed by the wall shear stress, as it advances with an average velocity that varies with respect to the length of the liquid layer. With increasing time, the liquid average velocity in the condenser increases. The liquid front will advance, until the heat pipe achieves its operational steady state, assuming sufficiently low parasitic heat leaks or applied heat loads. This model compared favorably with the microgravity experimental data presented by Brennan et al. [12], but it did not include effects of a parasitic heat load on the heat pipe. Also, this model did not account for the working fluid mass distribution and, therefore, it was not possible to estimate the liquid slug length observed by Brennan et al. [12].

Couto et al. [4,14] presented a one-dimensional model, which included the effects of the parasitic heat load over the cryogenic heat pipe supercritical startup. Also, the vapor pressure and density gradient of the working fluid were determined based on the temperature gradient and the total working fluid mass. The supercritical startup process described by Couto et al. [4,14] is very similar to that described by Yan and Ochterbeck [3], but it was shown that a subcooled condition can exist in the condenser before the condensation process starting, depending on the vapor pressure. The initial temperature of the heat pipe considered was above the critical temperature, and the boundary condition at the condenser region is a specified time-variable temperature. This condition is consistent with most experiments in the literature, which use cryocoolers to provide heat rejection at the condenser region. The remaining length of the heat pipe (adiabatic and evaporator regions) is considered to be under the influence of a radiative parasitic heat load. This parasitic heat load results from any radiation heat transfer between the heat pipe and the spacecraft structure and heat loads from the space environment (e.g., direct sun irradiation, earth emission, albedo, etc.) or any convective heat transfer.

Depending on the initial condition of the heat pipe [4,14], the working fluid at the condenser region may achieve a subcooled condition before that of a saturated condition. The analysis by Couto et al. [4,14] considers the two cases for the initial condition described by Couto [14], described briefly as follows: i) case 1, the initial specific volume of the heat pipe working fluid is $v_f \gg v_{crit}$, where this primarily is theoretical and is not easily realized in practice, as the

necessary volume of the vapor space would be orders of magnitude greater than the volume of liquid, which is typically not the case in actual heat pipes; ii) case 2, the specific volume is less or near the critical specific volume, or $v_f < v_{crit}$ or $v_f \sim v_{crit}$, where this case represents the majority of practical applications. Detailed descriptions of the thermodynamic processes and states for each case are given in Couto et al. [4].

The startup model presented by Couto et al. [4] compared favorably with the microgravity data presented by Brennan et al. [12]. The authors used this model to perform an analysis of the effect of parasitic heat loads on the supercritical startup and concluded that an excessive parasitic heat load could cause a partial startup of the heat pipe. Also, after a successful startup, when steady-state operation is reached, the excess mass of working fluid blocks part of the condenser region in microgravity environment, which decreases the heat pipe performance.

For additional validation of the startup process and the theoretical model presented by Couto et al. [4,14], ground tests of a nitrogen/stainless steel cryogenic heat pipe were performed. Although the model did not consider the effects of the gravitational field, the comparison provides good insight into the supercritical startup of cryogenic heat pipes.

Experimental Analysis

The experiment consisted of testing a nitrogen/stainless steel cryogenic heat pipe in a vacuum chamber using a liquid nitrogen cooled calorimeter to cool the condenser region [14]. The experimental setup allowed horizontal and tilt tests of heat pipes under a vacuum environment ($P_{abs} < 1 \times 10^{-2}$ mbar).

Experimental Facility

The experimental setup used for testing the stainless steel/nitrogen cryogenic heat pipe consisted of a horizontal vacuum chamber (1200 mm long, $\varnothing_{int}$ 200 mm) and a calorimeter (2.2 liters) through which liquid nitrogen flowed. Figure 1 shows the vacuum chamber schematic. To accommodate different heat pipe geometries, the calorimeter had an internal cavity with a diameter larger than the external heat pipe diameter. A brass sleeve filled the gap between the calorimeter and the heat pipe, to provide a prescribed temperature boundary condition at the condenser region. Additionally, another calorimeter (2.4 liters) was developed to allow direct contact between the liquid nitrogen and the heat pipe condenser section, providing more cooling capacity to the experimental setup.

The vacuum chamber was connected to an Edwards® RV8 rotary vacuum pump. The pressure in the vacuum chamber was monitored using an active pressure gauge Edwards® APG-M connected to an Edwards® AGD display. On one side of the vacuum chamber, a feedthrough for 36 T-type thermocouples and two pairs of electrical connections was used. The electrical connections allowed for the heat generation inside the chamber in future tests. On the other side of the vacuum chamber, a pair of feedthrough was connected where the liquid nitrogen (LN_2) flowed to the calorimeters. A vacuum relief valve also was installed on the plate. Two brass sleeves embraced the condenser region of the heat pipe, to fit inside the calorimeter.

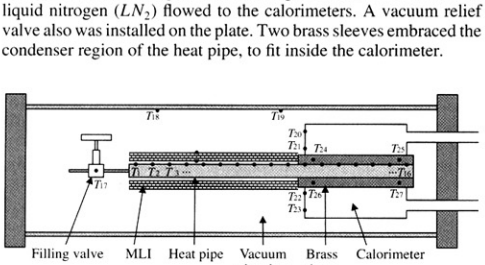

Fig. 1 Thermocouple positions.

Table 1 CryoNHP design summary (Couto [14])

Tube material: AISI 304 stainless steel	
Tube dimensions:	
Outer diameter	19.05 mm (3/4 in.)
Wall thickness	1.3 mm
Lengths:	
Evaporator	0.30 m
Condenser	0.30 m
Transport section	0.20 m
Nitrogen charge:	31.1 g
Maximum heat transport capacity:	2.2 W.m (at 82 K)
Wick structure:	Metal screen
Mesh	160
Number of layers	8
Thickness	1.676 mm

Heat Pipe Design Summary and Instrumentation:

The CryoNHP design has been given in detail by Couto [14] and is summarized in Table 1. The condenser region of the heat pipe was placed in the calorimeter, while the remaining length was covered with multilayer insulation (MLI) composed of ten layers of aluminum foils and nylon screens to minimize radiative parasitic heat loads. A Hewlett-Packard® 34970A Data Acquisition Unit was used to monitor 16 Omega® T-type AWG40 thermocouples that were installed on the external wall of the heat pipe (see Fig. 1). Also, the temperatures of the following items were monitored for future parameter estimation: fill valve of the heat pipe; vacuum chamber inner wall; outer and inner layers of the heat pipe MLI; brass sleeves; and calorimeter.

Uncertainty Analysis

The thermocouples were calibrated at two reference temperatures: ice point temperature at atmospheric pressure (273.15 K ≡ 0°C) using an Hg precision thermometer and saturation temperature of liquid nitrogen at atmospheric pressure (77.4 K). For the ice point temperature, the T-type thermocouples presented a random error of ±0.1 K and a systematic error of 0.2 K, whereas at nitrogen saturation temperature the readings were 73.8 ± 0.3 K, showing a systematic error of −3.5 K. The variation of the systematic error and random error between 273.15 and 77.4 K was considered linear:

$$\varepsilon_s = \left(\frac{0.2 - 3.5}{273.15 - 77.4}\right)(Y - 77.4) + 3.5 \tag{1}$$

$$\varepsilon_r = \left(\frac{0.1 - 0.3}{273.15 - 77.4}\right)(Y - 77.4) + 0.5 \tag{2}$$

where Y is the measured temperature as given by the data acquisition system. The corrected value of the measured temperature is given by

$$T = Y + \varepsilon_s \pm \varepsilon_r \tag{3}$$

where ε_s and ε_r are the systematic and random errors, respectively.

The measurement of temperature at cryogenic levels is very difficult as at such low temperature levels, the heat conduction along the thermocouple wires can affect the measured data. The data acquisition system was at ambient temperature and to minimize the heat conduction from the data acquisition system, the thermocouple wires were thermally grounded to the calorimeter. The heat conduction through the grounded thermocouple wires can be calculated by

$$Q_w = n_w \frac{\pi d_w^2 \Delta T}{4L}(k_{Cu} + k_{Co}) \tag{4}$$

For a temperature difference of 23 K between the calorimeter and the heat pipe, the heat transferred through the thermocouple wires is 1×10^{-3} W, whereas at 100 K the heat transport capacity of the heat pipe is 2 W. Therefore, the heat lost by conduction through the

thermocouple wires is less than 0.05% of the heat pipe transport capacity, thus being negligible.

Experimental Procedure

The experimental procedure consisted of cleaning, assembling, charging, and testing the heat pipe. First, the heat pipe container, metal screen, end caps, and filling tube were cleaned in ultrasonic cleaning equipment using trichloroethane for degreasing and solid particle removal. After cleaning, a passivation process was performed, which consisted of immersing the parts in a solution of 60% nitric acid and deionized water for 2 h. After passivation, the parts were wrapped in plastic to prevent contamination before assembly.

An AISI 316 stainless steel screen wick (mesh no. 160) was wrapped inside the heat pipe container to obtain a wick structure with four layers. The end caps and filling tube were welded to the container by a TIG (tungsten inert gas) process, where the heat pipe was filled with argon gas to prevent oxidation during the welding process. After welding, the heat pipe was cleaned again as described before. A Swagelok® needle valve was connected to the filling tube to seal the heat pipe after charging.

The heat pipe was charged with 99.99% pure nitrogen. The process was performed at room temperature or at liquid nitrogen temperature depending on the pressure level available from the supply system. Fluid charge was determined by weight, where the heat pipe was weighted after filling and compared with the empty weight. The difference provided the working fluid charge.

Testing consisted of cooling the heat pipe condenser to a temperature below the critical temperature of nitrogen. Initially, the heat pipe was at room temperature. The preparation for the test began with the evacuation of the vacuum chamber using the rotary pump. When the pressure was below 2×10^{-2} mbar, the data acquisition system was activated and the calorimeter was flooded with liquid nitrogen, cooling the brass sleeve and the condenser region. The temperature of the calorimeter was monitored constantly to avoid dryout, which would lead to a temperature increase of the condenser. The test was finished when the largest temperature variation observed was less than 1 K per hour (steady-state condition).

Results and Discussion

Numerous experiments were carried out as part of the overall test plan, where only those results, which highlight significant factors, are reported herein. The first test of the nitrogen/stainless steel heat pipe was performed and designated herein as test I, where this test was conducted with a fluid charge deficiency of approximately 30%. Theoretical results presented by Couto et al. [4,14] showed that a deficiency of working fluid charge might hinder the heat pipe from priming completely.

The condenser region of the heat pipe was fitted to the calorimeter using the brass sleeves, and the vacuum chamber was closed and evacuated to a pressure of 4×10^{-2} mbar which was the best vacuum quality obtainable with the given system. No MLI was used along the transport and evaporator sections of the heat pipe. At this point, the data acquisition system was activated, and the calorimeter was flooded with liquid nitrogen. After the flooding of the calorimeter, the pressure of the vacuum chamber increased to 0.1 mbar due to differential expansion of the LN_2 feedthrough at very low temperatures.

Figure 2 shows the first experimental data (symbols) for the temperature during the startup for different axial positions obtained for the CryoNHP. The theoretical data obtained with the model presented by Couto et al. [4,14] are also shown (lines) for the same axial positions. The parasitic heat load for this experiment was estimated to be $q_p = 3.90 \pm 0.55$ W. Two curves were plotted for each axial position: one for the maximum parasitic heat load estimated (4.45 W) and another for the minimum parasitic heat load (3.35 W).

The estimation of the parasitic heat loads was performed based on the steady-state temperature measurements and based on a network thermal resistances model presented by Faghri [2]. It was considered that the primed length of the device was working as a heat pipe

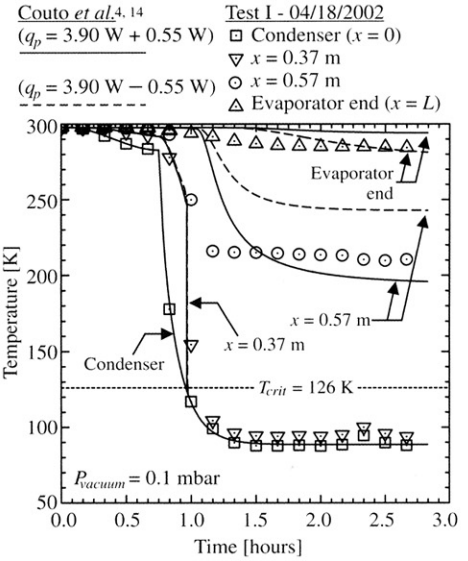

Fig. 2 Transient cooldown (test I).

transporting the heat conducted from the dry region and the radiative parasitic heat load as well:

$$Q_e = q_{\text{cond}} + q_p \tag{5}$$

Q_e can be estimated by using the network thermal resistance model [2] and the temperature difference measured between the liquid column edge $(Y|_{x=0.47\ \text{m}})$ and the condenser section $(Y|_{x=0})$. The heat conducted from the dry region, q_{cond}, was estimated using Fourier's law and the temperature gradient measured in the dry region at positions $x = 0.47$ m and $x = 0.52$ m is as follows:

$$q_{\text{cond}} = k_s A_s \left.\frac{\Delta Y}{\Delta x}\right|_{x=0.47} = k_s A_s \frac{(Y|_{x=0.52} - Y|_{x=0.47})}{(0.52 - 0.47)} \tag{6}$$

With the knowledge of the heat conducted from the dry region, q_{cond}, and the total heat load, Q_e, q_p can be obtained from Eq. (5).

It can be observed that the calorimeter was able to cool the condenser region below the nitrogen critical temperature in less than 1 h, and after 1.5 h the condenser achieved a steady-state average temperature of 82 K. Also, after 1.5 h, the heat pipe achieved a nonoperational steady-state condition, where only 58% of the entire length (0.47 m) was primed. Two possible reasons for this nonoperational condition can be listed:

The parasitic heat loads from the environment increased the temperature gradient of the heat pipe during startup, which was large enough to vaporize all the incoming working fluid at the liquid column leading edge under steady-state conditions ($x = 0.47$ m). Also, liquid was vaporized along the primed length of the heat pipe due to the parasitic heat load, reducing velocity of the liquid column. The combination of these two effects decreased the rewetting velocity to zero after 1.5 h of testing.

The fluid charge (~70% of the required fluid charge) was not sufficient to provide enough fluid for the liquid column to overcome the effects of the parasitic heat load, that is, there was insufficient working fluid to prime the heat pipe completely.

In fact, the working fluid mass of a heat pipe can be written in terms of the saturated liquid and vapor densities and of the liquid and vapor volumes:

$$m_f = \rho_\ell V_\ell + \rho_v V_v = \rho_\ell A_\ell L + \rho_v A_v L \tag{7}$$

Equation (7) provides m_f to prime completely a heat pipe with a defined geometry (L, A_ℓ, A_v) as a function of the saturation temperature [$\rho_\ell(T_{sat})$ and $\rho_v(T_{sat})$]. On the other hand, Eq. (7) can provide the maximum length L primed by a given working fluid mass as a function of the saturation temperature, which is shown in Fig. 3. The total length of the heat pipe being tested is shown with a dashed line. For this calculation, the working fluid mass in the dry region and the effects of the parasitic heat load were neglected for simplification. It can be observed that a heat pipe with a fluid charge deficiency would never prime completely. Also, it can be observed that an excess of 15% in the designed working fluid mass is required for the heat pipe to prime completely at 120 K.

Figure 4 shows the axial temperature profile during startup for different times. The model was able to predict the steady-state length of the liquid column as well as the steady-state axial temperature profile of the first experiment, but in general, it overestimated the transient temperatures during the startup process of the heat pipe. This is due to the model considering that any excess condensed liquid accumulates in the condenser as a liquid slug (microgravity environment). In ground tests, the capillary forces cannot support a liquid slug across the vapor channel diameter and the excess liquid spreads as a puddle and facilitates the priming of the heat pipe [12].

The excess working fluid during startup is shown in Fig. 5, which presents the liquid fill ratio for the test I experiment. The liquid fill is defined as the ratio between the condensed liquid mass m_ℓ and the mass that the wick structure can hold m_{wick}:

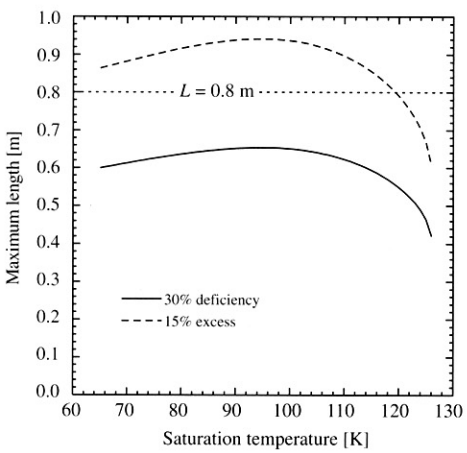

Fig. 3 Maximum primed length.

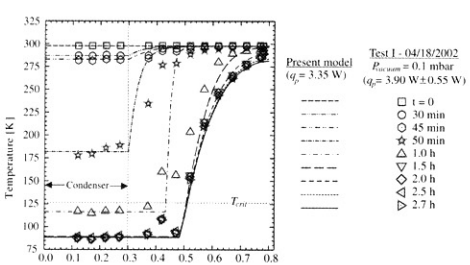

Fig. 4 Temperature profiles (test I).

$$N = \frac{m_\ell}{m_{wick}} = \frac{(1-n)A_c s/v_c}{A_{wick} s/v_\ell} \tag{8}$$

where n is the quality of the saturated fluid in the wetted region, A_c is the cross sectional area of the condenser (liquid + vapor), s is the position of the liquid column for a given time, A_{wick} is the cross sectional area of the grooves, and v_c and v_ℓ are the specific volumes of the saturated fluid in the wetted region and saturated liquid, respectively. If $N = 1$, the mass of liquid is enough to fill the wick with no excess liquid. For $N > 1$, excess liquid exists. The theoretical pressure-specific diagram for test I is shown in Fig. 6.

Another test (test II) followed with the same fluid charge in the heat pipe. In this test the transport and evaporator sections of the heat pipe were covered with MLI to decrease the parasitic heat loads. Figure 7 shows the comparison between the experimental and the theoretical temperature profiles for different times. The parasitic heat load estimated for this experimental run was $q_p = 2.95 \pm 0.49$ W. The theoretical curves shown in Fig. 7 are for the minimum parasitic

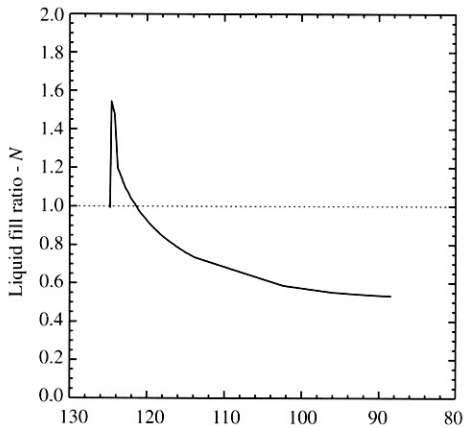

Fig. 5 Liquid fill ratio (test I).

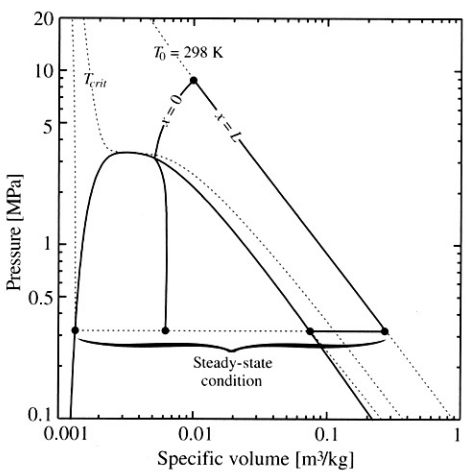

Fig. 6 Pressure-specific volume diagram (test I).

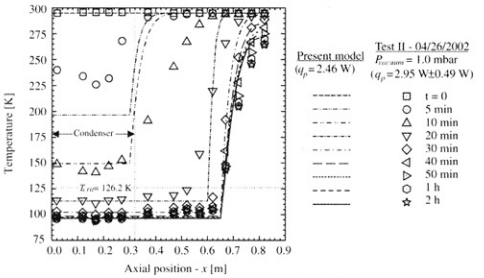

Fig. 7 Temperature profiles (test II).

heat load ($q_p = 2.46$ W). Once more, a nonoperational steady-state condition was observed after 1 h, but the liquid column primed 78% of the length of the heat pipe (0.62 m). Although the heat pipe was not fully primed, the improved insulation decreased the effects of the parasitic heat load, allowing the liquid column to advance further inside the heat pipe. With increased insulation, the effect of fluid charge deficiency seems to be more evident as the heat pipe could not prime completely. The model slightly overestimated the temperatures during transient operation, but it was able to reproduce the steady-state conditions (temperature distribution and liquid column length) with good accuracy. It is important to note that the model accounted for the experimental condition of undercharged mass of working fluid.

A third test (test III) was performed with similar conditions to those of test II. The objective of this test was to verify the repeatability of experimental results. The vacuum chamber pressure was greater than that of the second test (10 mbar), but the experiment showed good repeatability of results with the liquid column stagnating at $x = 0.61$ m.

For the next test (test IV), the heat pipe was charged with a 27% excess of working fluid. The transport and evaporator sections of the heat pipe were covered with MLI, but the fill valve was not. A thermocouple was installed on the fill valve to monitor its temperature relative to the heat pipe temperatures. The vacuum chamber was evacuated to a pressure of 2×10^{-2} mbar, and the acquisition system was activated. Then, the calorimeter was flooded with liquid nitrogen, where no change in the vacuum chamber pressure was observed. Figure 8 shows the experimental temperature at different axial positions along the heat pipe length as a function of time, which were obtained during this test. As the fill valve was not covered with MLI, there was a parasitic heat load (leak) from the valve to the heat pipe. To account for this parasitic heat load, experimental data of the temperature of the fill valve and of the evaporator end were used to estimate the conductive heat load coming from the valve. This conductive parasitic heat load (heat flux) was used in the model as the boundary condition at $x = L$, instead of the insulated boundary condition. As the variation of the evaporator end temperature and fill valve temperature were not linear, the conductive parasitic heat load incoming from the valve was obtained as a function of time.

The condenser temperature reached the critical temperature of nitrogen after 1.33 h, but the pressure model indicated that the vapor pressure decreased below the critical pressure only after 2 h, when the condenser temperature was at 118 K. The theoretical model indicates that the heat pipe would prime quickly (in 25 min) below 118 K, but on the other hand, the experimental data seem to indicate that there was no priming and the heat pipe was cooled only by conduction (see Fig. 9). Some possible reasons for the heat pipe startup failure are the following:

The vapor pressure never decreased below the critical pressure of nitrogen due to excess working fluid mass. To check this possibility, the experimental temperature data were used in the pressure model to calculate the vapor pressure during the startup. The results showed that the lowest vapor pressure achieved by the heat pipe during the fourth test was 4.1 MPa. In fact, this pressure is still 0.7 MPa greater than the critical pressure of nitrogen (3.4 MPa).

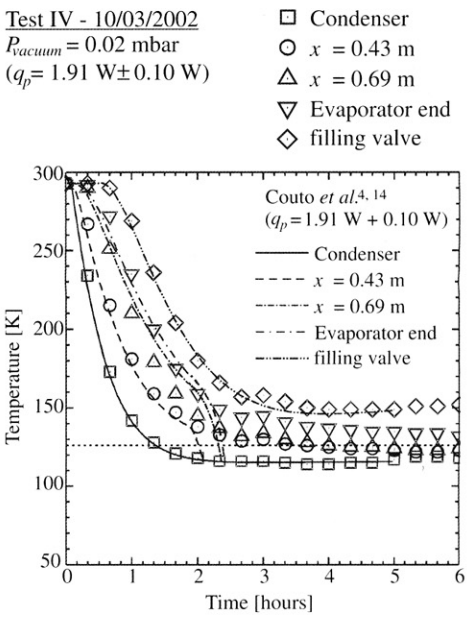

Fig. 8 Transient cooldown (test IV).

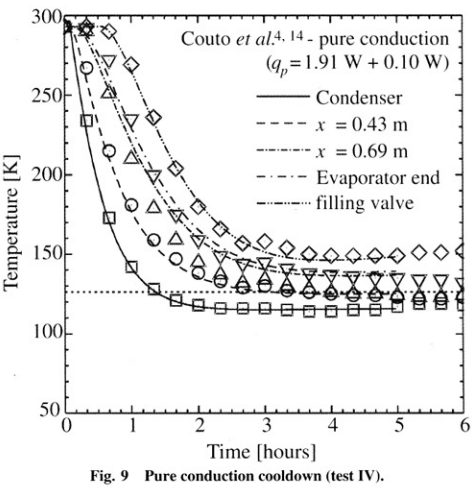

Fig. 9 Pure conduction cooldown (test IV).

The lowest temperature reached by the condenser was 116 K after 3 h of testing. This small saturation level provides a saturated liquid with a low latent heat, which makes it very sensitive to parasitic heat loads.

With increased vacuum level, contact resistance effects between the brass sleeves and the calorimeter provided less cooling capacity of the experimental apparatus.

The last statement can be verified as follows: the pressure inside the vacuum chamber during this experiment was 2×10^{-2} mbar, or 100 times lower than the pressure of the first experiments. In this

rarefied atmosphere any effect of convection over the heat pipe startup can be neglected. With the low vacuum levels of the first tests, the atmosphere inside the vacuum chamber was cooled by the calorimeter, which has a large thermal mass, improving the heat transfer from the calorimeter to the sleeve, and to the heat pipe condenser.

To check this explanation, the rotary pump of the vacuum chamber was turned off after the nonoperational condition was achieved. The pressure in the vacuum chamber increased quickly to 6×10^{-2} mbar in less than 1 min, to 2×10^{-1} mbar in 5 min, and to 1 mbar after 15 min remaining stable around this value for 1 h. The temperature profiles of the heat pipe for this test are shown in Fig. 10. It can be observed that the local temperatures of the heat pipe decreased after the shut down of the rotary pump (6 h) due to improved convection inside the vacuum chamber. At cryogenic temperature levels, the heat pipe was very sensitive to small heat loads, even those provided by a rarefied atmosphere.

Another test (test V) followed with the same setup. The same startup failure was observed showing that the calorimeter was not

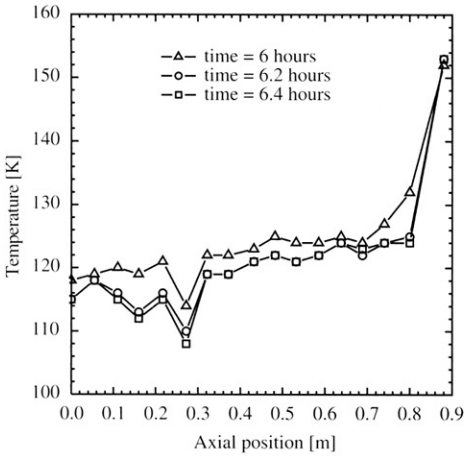

Fig. 10 Temperature profiles after rotary pump shut down (test IV).

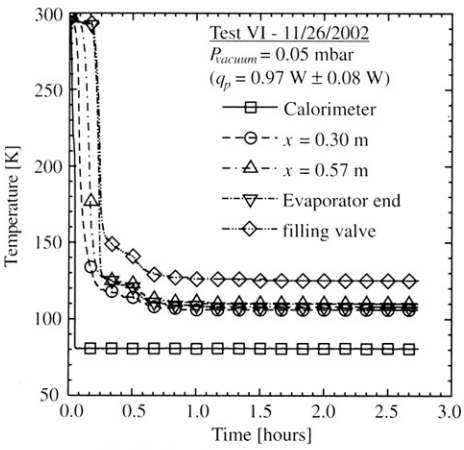

Fig. 11 Transient cooldown (test VI).

able to provide enough cooling to the condenser regions of the heat pipe. The experiment presented good repeatability with the same temperature level achieved by the heat pipe in test IV. After the test V, the experimental setup was disassembled and the second calorimeter was installed. The second calorimeter allowed liquid nitrogen to be in direct contact with the condenser wall of the cryogenic heat pipe, thus providing a larger cooling capacity.

A next experiment (test VI) was performed with the second calorimeter. The second calorimeter provided increased cooling to the heat pipe and resulted in a successful startup where the total length was primed by the liquid column. The calorimeter imposed an abrupt cooling of the condenser, producing a fast transient. According to the experimental data the heat pipe was primed in less than 15 min (which means a variation of 14 K/s in the condenser section, and a 0.2 K/s in the evaporator end). The numerical solution of the model was not able to reproduce the fast transient due to the large temperature gradient at the leading edge of the liquid column caused by the abrupt cooling of the condenser region. As the temperature of the condenser decreased quickly, the theoretical average liquid column velocity increased quickly, which in turn, provided a long liquid column length. The long length obtained produced a large temperature gradient at the liquid column interface, which pushed back the liquid column, causing the iterative process to diverge. Several time steps were tried, but the solution continued to diverge. Therefore, no comparison between theoretical and experimental data was possible for this experiment. Figure 11 shows the transient cooldown experimental data. The condenser region was cooled to the critical temperature of the nitrogen in less than 3 min, and the cooling effect spread over the heat pipe in less than 15 min. The heat pipe reached a steady state after 45 min of testing, with the condenser region at a temperature around 80 K, and the remaining length at 108 K. The fill valve was slightly higher than the rest of the heat pipe and was at 125 K.

Conclusions

The experimental data and theoretical model provided good insight into the supercritical startup of cryogenic heat pipes with the following conclusions:

1) Cryogenic heat pipes are very sensitive to parasitic heat loads. The rewetting process is controlled by the conducted heat flux from the dry region of the heat pipe. Any parasitic heat loads increase the temperature gradient in the dry region, increasing the heat conduction to the liquid column. Also, parasitic heat loads vaporize the fluid along the liquid column, thus decreasing the average liquid velocity. These effects combined decrease the liquid column momentum, and the rewetting process may stagnate before the heat pipe is fully primed for relatively small parasitic heat loads. Additionally, parasitic heat loads may add loads to the heat pipe on the order of the maximum heat transport capability.

2) An excess fluid charge will cause an increase of the vapor pressure of the heat pipe. Depending on the combination of parasitic heat loads and excess fluid charge, the vapor pressure may never decrease below the critical pressure of the working fluid, even if the condenser is at a temperature below the critical point. A working fluid deficiency will decrease the vapor pressure during startup, but the total working fluid amount may not be enough to prime the heat pipe completely.

3) A fast cooling rate of the condenser will cause a large temperature gradient on the dry region of the heat pipe. This will push a large amount of working fluid to the condenser region, which will turn into subcooled liquid before condensation begins. As the heat pipe continues to cool down, the subcooled liquid will transition into saturated fluid at a temperature far below the critical point, which will produce a liquid column with a considerably large momentum, facilitating the priming of the heat pipe

Acknowledgements

The authors would like to acknowledge the Brazilian Space Agency–AEB, CAPES Foundation, Brazilian Council of Research

and Development–CNPq, Clemson University, and the Federal University of Santa Catarina for supporting this project.

References

[1] Peterson, G. P., *An Introduction to Heat Pipes—Modeling, Testing and Applications*, 1st ed., Wiley, New York, 1991.

[2] Faghri, A., *Heat Pipe Science and Technology*, Taylor and Francis, Washington, D.C., 1995.

[3] Yan, Y. H., and Ochterbeck, J. M., "Analysis of Supercritical Start-Up Behavior for Cryogenic Heat Pipes," *AIAA Journal of Thermophysics and Heat Transfer*, Vol. 13, No. 1, Jan./March 1999, pp. 140–145.

[4] Couto, P., Ochterbeck, J. M., and Mantelli, M. B. H., "Analysis of Supercritical Start-up Limitations for Cryogenic Heat Pipes with Parasitic Heat Loads," *AIAA Journal of Thermophysics and Heat Transfer*, Vol. 19, No. 4, 2005, pp. 497–508.

[5] Röster, S., Groll, M., Supper, W., and Konev, S., "Analysis and Experimental Investigation of a Cryogenic Methane Heat Pipe," *Proceedings of the 16th Intersociety Conference on Environmental Systems*, July 1986, pp. 352–355.

[6] Ochterbeck, J. M., Peterson, G. P., and Ungar, E. K., "Depriming/Rewetting of Arterial Heat Pipes: Comparison with Share-II Flight Experiment," *AIAA Journal of Thermophysics and Heat Transfer*, Vol. 9, No. 1, Jan./March 1995, pp. 101–108.

[7] Joy, P., "Optimum Cryogenic Heat Pipe Design," ASME Paper 70-HT/SpT-7, June 1970.

[8] Peng, X. F., and Peterson, G. P., "Acceleration Induced Depriming of External Artery Heat Pipes," *AIAA Journal of Thermophysics and Heat Transfer*, Vol. 6, No. 3, 1992, pp. 546–548.

[9] Couto, P., and Mantelli, M. B. H., "Cryogenic Heat Pipe—A Review of the State-of-the-Art," *Proceedings of the Brazilian Congress of Thermal Engineering and Sciences* [CD-ROM], Oct. 2000.

[10] Brazilian Space Agency, *PNAE—Brazilian Policy for Space Activities* (original in Portuguese), AEB, Brasilia, DF, Brazil, 1996.

[11] Colwell, G. T., "Prediction of Cryogenic Heat Pipe Performance," NASA Final Rept. NSG-2054, March 1977.

[12] Brennan, P. J., Thienen, L., Swanson, T., and Morgan, M., "Flight Data for the Cryogenic Heat Pipes (CRYOHP) Experiment," AIAA Paper 93-2735, July 1993.

[13] Rosenfeld, J. H., Buchko, M. T., and Brennan, P. J., "A Supercritical Start-Up Limit to Cryogenic Heat Pipes in Microgravity," *Proceedings of the 9th International Heat Pipe Conference*, Vol. 2, 1995, pp. 742–753; also Paper 860962.

[14] Couto, P., "Theoretical and Experimental Analysis of Supercritical Startup of Cryogenic Heat Pipes," Ph.D. Thesis, Mechanical Engineering Department, Federal University of Santa Catarina, Florianopolis, Brazil, March 2003.